Bionic Optimization Design of Electronic Nose Chamber for Oil and Gas Detection

Zhiyong Chang - Southwest Jiaotong University; Jilin University
Youhong Sun - Jilin UniversityCorresponding Author
Yuchen Zhang - Southwest Jiaotong University; Jilin University
Yanli Gao - Clinical Medicine, Bethune First Hospital of Jilin University, 130021, Changchun, China
Xiaohui Weng - Jilin University
Donghui Chen - Southwest Jiaotong University; Jilin University
Liewe David - University of Gloucestershire
Jun Xie - Southwest Jiaotong University; Jilin University; Air Combat Service Academy, Air Force Aviation University, 130021, Changchun, China

Journal of Bionic Engineering 15 (2018) 533–544 DOI: https://doi.org/10.1007/s42235-018-0044-6

Abstract

In this paper, a miniaturized bionic electronic nose system is developed in order to solve the problems arising in oil and gas detection for large size and inflexible operation in downhole. The bionic electronic nose chamber is designed by mimicking human nasal turbinate structure, V-groove structure on shark skin surface and flow field distribution around skin surface. The sensitivity of the bionic electronic nose system is investigated through experimentation. Radial Basis Function (RBF) and Support Vector Machines (SVM) of 10-fold cross validation are used to compare the recognition performance of the bionic electronic nose system and common one. The results show that the sensitivity of the bionic electronic nose system with bionic composite chamber (chamber B) is significantly improved compared with that with common chamber (chamber A). The recognition rate of chamber B is 4.27% higher than that of chamber A for the RBF algorithm, while for the SVM algorithm, the recognition rate of chamber B is 5.69% higher than that of chamber A. The three-dimensional simulation model of the chamber is built and verified by Computational Fluid Dynamics (CFD) simulation analysis. The number of vortices in chamber B is fewer than that in chamber A. The airflow velocity near the sensors inside chamber B is slower than that inside chamber A. The vortex intensity near the sensors in chamber B is 2.27 times as much as that in chamber A, which facilitates gas molecules to fully contact with the sensor surface and increases the intensity of sensor signal, and the contact strength and time between odorant molecules and sensor surface. Based on the theoretical investigation and test validation, it is believed that the proposed bionic electronic nose system with bionic composite chamber has potential for oil and gas detection in downhole.

Keywords: electronic nose, bionic chamber, sensors, oil gas detection

1. Introduction

In the process of oil and gas detection, it is very important to discover and determine the specific location of oil and gas reservoirs. At present, the most commonly used methods for oil and gas detection are sidewall coring[1], electrical measurement[2] and gas chromatography analysis[3] where these technologies have been tried and tested on the well. However, the hysteresis and interference of upward oil and gas cannot be effectively eliminated because of the processes from the under- ground to the surface. Hence it is difficult to solve the problems of timeliness, continuity and quantification. Therefore, the quality of oil and gas detection and analysis is poor and the formation of oil and gas content cannot be effectively reflected[4]. The fluid and gas detection technology in drilling can be used to discover the underground position of oil and gas in time[5]. Among the fluid and gas detection technologies, electronic nose system has attracted many research and application interests. Electronic nose system comprises an array of electronic chemical sensors with partial specificity and an appropriate pattern recognition system and is capable of recognizing simple or complex odours. It has been widely used in food science[6], medical science[7], agricultural science[8], and environmental monitoring[9] in recent years. Electronic nose can meet the real time and accuracy requirements of oil and gas detection to some extent for the characteristics of fast detection speed, wide range of measurement and evaluation. At the same time, a series of achievements in oil and gas drilling, sampling and oil gas separation have also provided the basis for the use of electronic nose to detect underground oil and gas resources[10]. However, due to the narrow downhole space and complex environment, the detection system have to be small and sensitive. Electronic nose system is inspired by the olfactory perception system of organisms as the performance of biological olfaction depends on some variables, such as the nasal structure, the number of olfactory cells and the diffusion of odour molecules in the air and mucous membranes[11], so changing the internal structure or volume of the nasal cavity will significantly improve the olfactory function[12]. Therefore, the structural design of the electronic nose chamber, which mimics the structure and function of the nasal cavity, has an important effect on the miniaturization, sensitivity and stability of the electronic nose system[13]. Recently, many scholars have been working on the design of electronic nose chamber to improve the performance of electronic nose system. Francesco *et al*. designed a measurement chamber

for the dynamic exposure of a sensor array to gaseous or liquid samples. The chamber is designed to have flow distributors with the same size and radial symmetry so that each sensor in the chamber can obtain the same sample concentration and sample flow rate. The device was designed to optimize sensor response signals in terms of stability, reproducibility, response time and amplitude[14]. Viccione *et al*.[15] pointed out that elec- tronic nose chamber plays an important role in the sampling process in which the sensor position strongly affects the response of the system. The key to the design of related geometries is to ensure that the injected volatile sample reaches a stable and uniform state in the cavity at the fastest possible time and minimize the presence of detention and/or recirculation zones. Therefore, in order to increase the contact surface of the volatile sample and the sensors, the fluid dynamic study of a cylindrical sensor chamber was proposed and a 3D model of the sensor chamber was developed to solve the transport equations of both momentum and mass[15]. The fluid dynamics of the chamber was analyzed to ensure uniform flow conditions. It can be seen that most re- searches focused on the analysis of fluid flow characteristics whilst little was considered about the effect of optimal design of inner chamber structure on fluid flow characteristics. There is a lack of specific optimization, comparison and improvement of the electronic nose chamber. However, the previous design idea of the chamber provides a reference for the proposed chamber design in this paper.

The development of bionics provides an effective new way for engineering problem solving and techno- logical breakthrough and a new idea for the design of structural characteristics, surface morphology and size of microstructures. Researches show that the application of bionic research to the design of flow field control can effectively improve the performance and efficiency of the system[16,17]. At present, most studies of artificial olfactory are limited to the sensors mimicking olfactory cells and array optimization[17,18] and the pattern recognition algorithm of biological analysis and recognition[16,19]. However, the nasal cavity structure, the diffusion of gas molecules and the layout of the sensor array have significant influence on the performance of small and micro-gas-sensing detectors under special working conditions. As far as authors are aware, this is area that should be further investigated. It has been demonstrated that the structural changes of key olfactory areas have significant effect on the sensitivity of olfactory sensitive cells in which fluid structure is a key factor in the diffusion and retention of odour molecules in olfactory regions[20,21]. These provide a basis for the

bionic optimization design of the electronic nose chamber structure where whole nasal cavity of human is dome-shaped from anterior to posterior, and the middle section is horizontal. The posterior section is curved at an angle of 30 degrees from the top of the nose to the bottom. When air flows in from the nostril, it enters the main nasal cavity through the nasal valve with the smallest cross-sectional area. After the gas enters the nasal cavity, it stays in there for a long time, which makes the odorant and the olfactory receptor in full contact to enhance the olfactory ability. The main reason for this phenomenon is that the cross-sectional area of the nasal cavity is much larger than that of the nostril[22]. That is to say, the sensitivity of human sense of smell is not only related to the type and distribution of olfactory sensory cells and nerve responses, but also to the structure of the nasal cavity[23]. The changes of the olfactory region and the flow channel, especially in the cavity, strongly affect the olfactory sense of smell[24]. According to the bionic inspiration, the airflow velocity in the cavity can be adjusted, the shape of the gas flow passage should be small in front and big in back. In this situation, the turbulence can be formed in the gas flow passage, so that the sensor and the gas substance can contact as fully as possible. In the normal nasal cycle, turbinates have a rhythmic expansion and contraction, so that the airflow in the nasal cavity changes, which has a great impact on the olfactory function[24]. The turbinate structure can guide the airflow into the nasal cavity, allowing more gas to reach the olfactory area, and further enhance the ability to smell[25]. Therefore, the analysis of the influence factors of olfactory is based on the structural features of the nasal cavity and hydrodynamic characteristics of airflow in the nasal cavity, which can provide theoretical support and design inspiration for the design of electronic nose chamber structure. The internal structure of the gas chamber combines the structure of the nasal bones and the spoiler, which is conducive to the turbulence of the gas chamber and prolongs the residence time of the gas in the gas chamber. Meanwhile, the design of the bulk- head can form a diversion area, which facilitates the turbulent flow in the sensor array area and result in a full contact between the sensor array and the smell[25]. Based on the structural characteristics of human olfactory system, Wen *et al*. established a three-dimensional nasal cavity simulation model and the effects of the structural characteristics of the turbinate and the hydrodynamic characteristics of the airflow inside the nasal cavity on the olfaction were analyzed. This research provided the simulation basis for the ideal chamber design of sensor to collect odour signals steadily[25].

According to previous research[2], the introduction of the turbinate structure in the cavity makes the structure of the cavity more complicated, which increasesthe resistance of the fluid flow to a certain extent, decrease the fluid flow rate, and therefore affecting the detection sensitivity of the sensor. This resulted in the introduction of some bionic composite structures into the interior surface design of the fluid chamber may effectively reduce the resistance caused by the unnecessary added complicated structure. Sharks have very little resistance when swimming in water as its body is streamlined and the skin surface is also regularly distributed with many shield scales. On the surface of each scale, there are V-shaped micro grooves regularly arranged along the flow direction. This changes the fluid structure of the fluid boundary layer in the shark surface, which can effectively delay or inhibit the transformation of turbulence, thus effectively reducing the fluid resistance of sharks during swimming[26]. The successful application of the bionic structure inspired by shark skin in surface fluid research was presented[27]. This led to the intro- duction of the V-groove composite structure which can be used to reduce frictional resistance, and the friction between the wall of the chamber and the gas to be measured where to some extent, it can also reduce the vibration effect of the sensor.

In this paper, a novel chamber structure of electronic nose is designed inspired by turbinate structure of human combined with the V groove structure of shark skin. The characteristics of olfactory activity in human with sensitive olfactory ability was mimicked by the turbinate structure. In order to effectively reduce the adverse effect of the increase of fluid flow resistance in the chamber caused by the structure of the turbinate, the inner surface of the chamber and external surface of the bionic turbinate were prepared with V groove structure inspired by the shark skin surface. The structure optimization design method is applied in the whole cavity according to the environment and characteristics of oil and gas detection. The effectiveness and accuracy of bionic composite structure of the bionic electronic nose chamber are verified through comparative experiments. It may provide the theoretical support and experimental foundation for the future application of bionic electronic nose system in downhole oil and gas detection.

2. Method

2.1 Chamber design

2.1.1 Common chamber design

According to the fluid mechanics formula:

$$Q = vs, \qquad (1)$$

where, Q represents the fluid flow ($m^3 \cdot s^{-1}$), v represents the fluid velocity ($m \cdot s^{-1}$), and s represents the cross-sectional area (m^2). In the case of constant flow Q, the sudden increase of the cross-sectional area s will reduce the flow rate, so that the gas can stay longer in the nasal cavity. According to this characteristic, the common chamber structure is designed with "microstome and big cavity". The ratio of the maximum cross-sectional area to the minimum cross-sectional area of nasal cavity in normal adults is between 6.9 and 10.9[28]. Considering the sensor base layout and the flexibility of the electronic nose chamber in different environments, the chamber of the electronic nose was designed as a circular cross section, and the ratio of the maximum cross-section to the minimum cross-section radius was between 2.6 and 3.3. In order to miniaturize the electronic nose system for subsequent integration with the drill bit, and allow the electronic nose chamber to be connected to the gas cylinder trachea and valve, the minimum cross-sectional diameter was set to 16 mm. In normal adults, the length of the nasal passage was about 100 mm. Considering the arrangement of sensors in the electronic nose chamber (Figaro Engineering Inc-2000 series sensors, Japan) and miniaturization structural design features, the minimum length of the electronic nose chamber was determined to be 102 mm. The orthogonal test method was used to determine the size of bionic chamber of electronic nose[29]. Four fac- tors of bionic chamber were investigated, including the ratio of maximum to minimum cross-section radius (A), the length of chamber (B), the flow rate of sampling gas (C) and the sampling time (D). Based on these, 4 factors and 3 levels of $L_9(3^4)$ orthogonal test factors were established, as shown in Table 1 and Table 2.

The maximum response value detected by electronic nose was taken as the index, and the variance analysis and factor significance test were carried out with SPSS statistical software.

Table 1 Factors and levels

Level	Factor			
	A	*B* (mm)	*C* ($m \cdot s^{-1}$)	*D* (s)
1	2.8	102	0.5	60
2	3.0	120	0.8	90
3	3.2	128	1.2	120

Table 2 Test design data analysis

Variance source	Sum of deviation square	Mean square	*F* test value
A	0.196	0.121	5.132
B	0.061	0.054	1.194
C	0.114	0.081	3.167
D	0.002	0.023	0.023

The electronic nose was used to detect the odour of different samples, and each sample was repeated three times, then the average value was obtained. From the variance analysis, the influence degree of each factor on the maximum response value of electronic nose detection was A > C > B > D. By com- paring different detection conditions, the optimal com- bination of detection conditions was $A_2B_1C_2D_1$, that is, the ratio of the maximum cross-section to the minimum cross-section radius of the electronic nose chamber was 3, the length of the electronic nose chamber was 102 mm, the sampling gas flow rate was 0.8 $m \cdot s^{-1}$, and the sampling time was 60 s. Fig. 1 shows the common electronic nose chamber A. The chamber shell was obtained by 360 degrees rotation of three lines along the longitudinal axis, including a straight line at the front section, a curve at the middle section and a straight line at the back section. The wall thickness was 2 mm. The total length of the bionic chamber shell was 102 mm. The length of the front section was 5 mm. According to the shape of the outer wall of the bionic prototype of adult nasal passage, the middle curve is determined by the connection of two circular arcs whose radii were 38 mm and 40 mm. The length of the back section was 48 mm. TGS series gas sensor (Figaro Engineering Inc-2000, Japan), which is sensitive to the composition of gas components, was selected according to the characteristics of downhole volatile gas. Six sensors were fixed to the circular base, and the hole diameter was 8 mm.

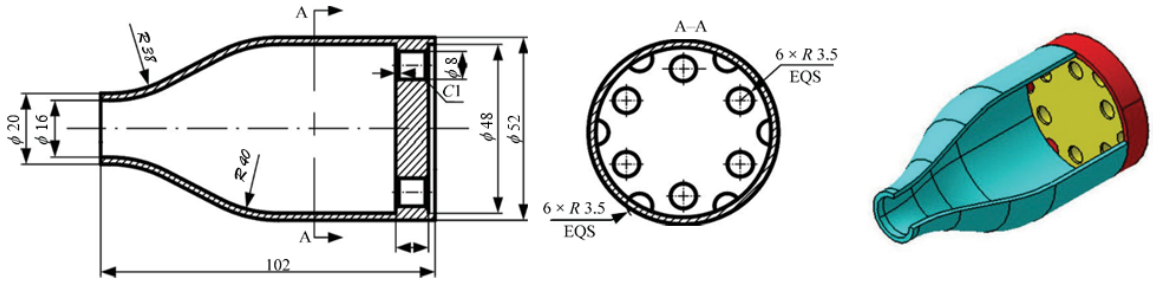

Fig. 1 The common nasal chamber A.

2.1.2 3D model reconstruction and flow field analysis validation

The nasal cavity scanning and 3D model reconstruction were performed on healthy adult males. The nasal cavity model was constructed by using MIMICS software with the smooth factor of 0.5. The optimal olfactory channel model was established, and the mesh number was 12256050. The optimized mesh model was fed into Fluent 6.3 to calculate the flow field of the nasal cavity model, and the flow field data of the CFD model were obtained during calm inspiration. Fig. 2 shows the velocity profile of steady-state inspiratory airflow of the nasal cavity in Fluent, which reflects the specific distribution of airflow velocity in the nasal cavity model. From the Reynolds number formula, in the nasal cavity, except the flow velocity, the other parameters of the model can be approximated as constant under the model setting condition. Due to that the olfactory receptor sites are confined in a relatively protected area of the nasal passage, it is possible that the transport of volatile chemicals to the olfactory receptor sites is critically dependent on the exact location of the maximum airflow velocity in the region of the olfactory epithelium[22]. The olfactory receptor sites are just the areas where the maximum velocity appears, that's where the turbulence is most likely to occur. It was verified that the airflow near the olfactory region must be turbulent to be perceived by olfactory cells, which provides a theoretical support for the placement of the sensor array and the structure design of the diaphragm and spoiler for the next electronic nose study.

2.1.3. Bionic chamber design

The engineering design of the integrated system, the straight spoiler structure which is similar to the structure of turbinate was added to the basis of the common chamber A. As the structure of human nasal turbinate is separated into the upper, middle and lower three channels, the bionic electronic nose chamber was divided into 6 regions using the clapboard. The clap- board acts as the nasal septum. Two spoilers were separately placed on the two sides of each clapboard, which is inspired by the turbinate structures of different human nasal cavity[14] where the proportion of the spoiler structure needs to be considered.

The bionic composite chamber B consists of shell, support column, clapboard assembly, base assembly, and sensor group. The base assembly was fixedly connected with the right end of the rear section of the bionic chamber shell. The top circle of the half conical frustum in the base assembly was fixed to the right end of the support column. The inner end of the six septa in the clapboard assembly was fixed to the cylindrical surface of the cylinder of the supporting column, and the outer end of the six septa was fixed and connected with the inner wall of the rear section of the bionic chamber shell. At the same time, the V-shaped groove structure inspired by the shark skin surface was designed on the inner wall of the chamber, and the surface of clapboard and spoiler. The V-shaped groove structure of shark skin is shown in Fig. 3.

The main dimensions of the support column, clapboard and spoiler were determined by orthogonal test[29]. Six factors were investigated, including the length of the support column (E), the diameter of the support column (F), the length of the clapboard (G), the width of the spoiler (H), the length ratio of upper and lower spoilers (I) and the length of the regular triangle V-shaped groove (J). Table 3 is the factor level table of $L_9(3^6)$ orthogonal test of six factors and three levels. The maximum response value detected by electronic nose was taken as the index, and the variance analysis and factor significance test were carried out by SPSS statistical software. The parameter setting was the same as that of the orthogonal test. By the comparison of different detection conditions, the optimal combination of detection conditions was $E_2F_1G_2H_1I_1J_1$, the length of the support column was 65 mm, the diameter of the support column was 10 mm, the length of the partition was 25 mm, the width of the spoiler was 10 mm, the length ratio of upper and lower spoilers was 1:2 and the length of the

regular triangle V-shaped groove and slot spacing were equal, both 0.5 mm. The specific design of the bionic composite chamber is shown in Fig. 4.

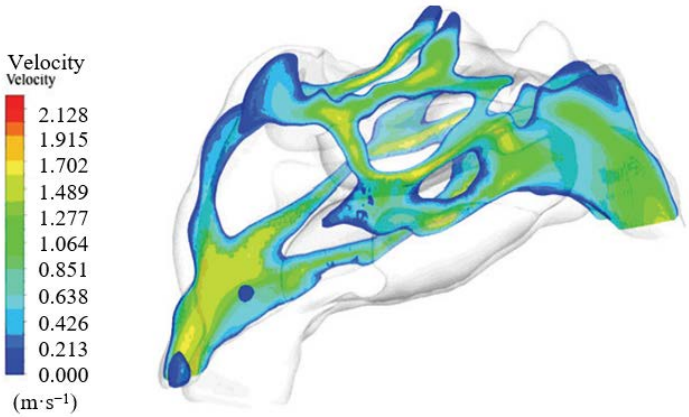

Fig. 2 The velocity profile of nasal steady inspiratory air flow.

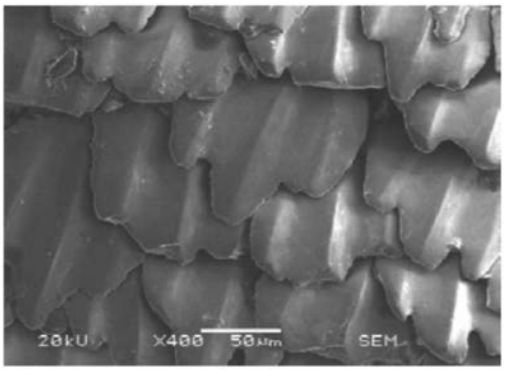

(a) 400 rate

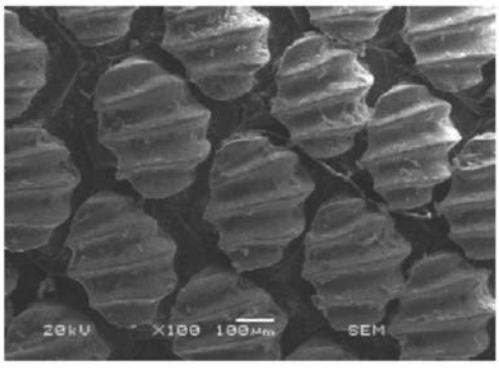

(b) 100 rate

Fig. 3 SEM photographs of the surface microstructure of shark skin[30].

Table 3 Factor and level

Level	Factor					
	E (mm)	F (mm)	G (mm)	H (mm)	I	J (mm)
1	60	8	15	10	0.5	0.3
2	65	10	20	12	1	0.5
3	70	12	25	14	2	0.8

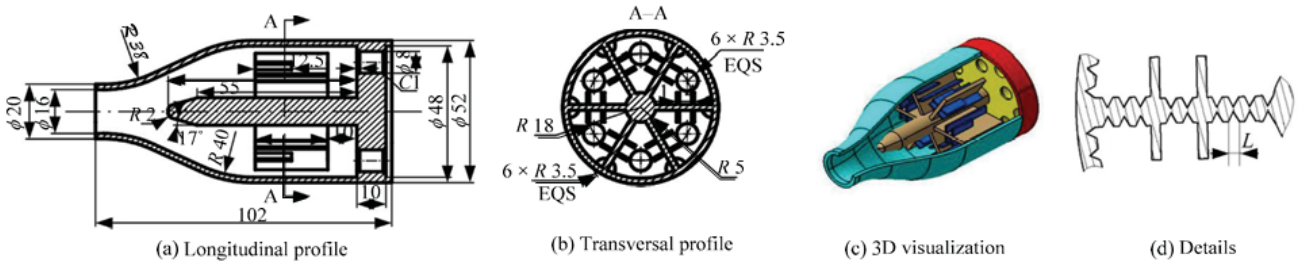

(a) Longitudinal profile (b) Transversal profile (c) 3D visualization (d) Details

Fig. 4 Electronic nose chamber B with biomimetic composite structure.

2.2 Sample implementation and electronic nose test

The proposed design of the electronic nose chamber model was built with ABS plastic using a 3D printer, Project 5500 (3D System Corp, USA) 3D printer. The materials were ABS plastic and the printing accuracy was 750 × 750 dpi. The sample is shown in Fig. 5. Its dimension accuracy is ct7–ct8, and the roughness R_a is 32 μm. The machining quality of the circular holes on the edge and the inner cavity of the printed bionic chamber model is better, which can meet the usage requirement.

The test sample gas was collected from mines in the oil shale producing area of Nongan County, Jilin Province, China. The high temperature nitrogen gas was continuously injected into the mine, and the bottom hole temperature was slowly increased. The bottom gas was collected at five different temperatures. A total of 165 bags of sample gas were collected, with 500 ml per bag. GC7890A/MSD5975C gas chromatography-mass spectrometry (Agilent Technologies, USA) was used to test one bag of sample gas at each temperature. The detection results show that the sample gas is mainly composed of nitrogen, carbon dioxide, hydrocarbon gas, sulfide and other 13 kinds of gas, and the composition and content of volatile substance of pyrolysis gas at different temperatures are different. With the increase of temperature, the content of nitrogen and carbon dioxide decreased gradually, and the

content of hydrocarbon gas and sulfide increased gradually. Six gas sensors were selected to determine which were the more sensitive to the gas composition using the Figaro TGS2602, TGS2610, TGS2611, TGS2442, TGS2620, TGS2612, 2000 series gas sensor. According to the test results, the TGS2610, TGS2611 and TGS2620 sensors have good response to the mixed gas. Considering the complexity of downhole detection conditions, which may lead to sensor damage, three kinds of sensors were selected to be placed on the base of the chamber. For each kind of sensor, two sensors were used for test. A total of six sensors were assembled for the sensor array to carry out the final test. The bionic electronic nose system used in the test includes air pump, electromagnetic valve, gas mass flow controller, electronic nose and bionic chamber, filter noise reduction circuit, data acquisition instrument, computer and so on. The system composition is shown in Fig. 6.

The signal generated by the sensor was collected by the data acquisition system, and transmitted to the PC computer for processing. Each electronic nose chamber was tested with 4 groups of different entrance velocities in a clean air laboratory. The temperature in the laboratory was 22 ˚C ± 1 ˚C, and the humidity was 60% ± 1%. At the beginning of the test, the first chamber was placed at the base of electronic nose sensor. The electronic nose system was preheated and cleaned until the sensor reached a stable state. The flow valve was used to control the speed of gas flow, so that the speed of the gas met the test requirements. The signal acquisition system was used for data acquisition. After the data collection was completed, clean air was injected into the electronic nose chamber for cleaning before the next test was carried out as shown in Fig. 7.

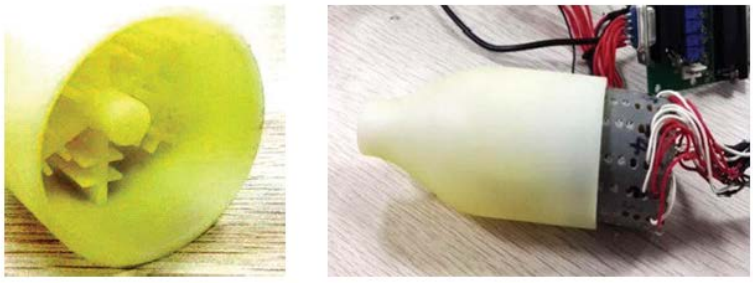

(a) Electronic nose chamber (b) Installation schematic diagram

Fig. 5 Electronic nose chamber sample and installation schecmatic diagram.

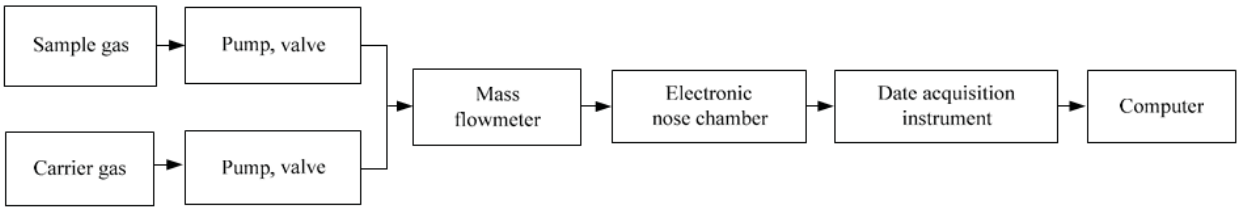

Fig. 6 Working flow chart of electronic nose system.

Fig. 7 The experimental system of the electronic nose system.

3. Results and discussion

3.1 The sensor response analysis of different chambers

In the multivariate test of the improved electronic nose chamber, the sensor did not respond immediately when the sample gas was injected. The response time was greatly affected by the sensitivity of the bionic electronic nose system. For the same electronic nose chamber, the response time of the sensor was changing with different inlet velocities, it was corresponding to the changes of airflow in human nasal cavity. If the air velocity was low, the gas flowed slowly. If the time to reach the olfactory area increased, and it was difficult to generate small gas eddies. The gas molecules cannot fully contact with the odour receptors. If the gas flow rate was too high, the residence time of gas molecules in the odour receptor

was too short to produce the best olfactory effect. To further investigate the effect of the two different chambers on the electronic nose system, the data were normalized and the response curves of the three most responsive sensors in the two chambers were plotted. As shown in Fig. 8, the response speed of the three Figaro sensors TGS2610, TGS2611 and TGS2620 in the proposed bionic system chamber B was greater than that of the common chamber A. This was because that the added spoiler structure increased the flow resistance in the cavity. Due to the V shaped groove structure on the inner surface, the friction resistance was reduced. Meanwhile, because of the different length of spoiler and the annular groove structure at the bottom of support column, the gas turbulence was produced on the sensor surface. Consequently, the gas residence time was relatively increased, and the detection accuracy was improved to a certain extent. It was proved that the detection sensitivity of the bionic composite chamber B was higher than that of the chamber A.

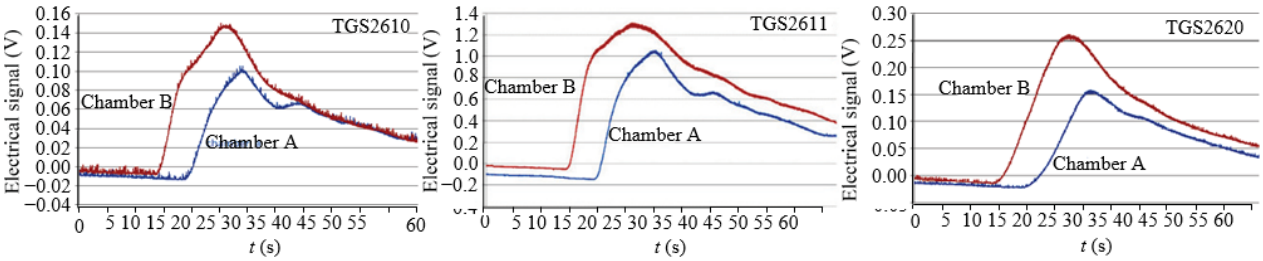

Fig. 8 Response diagram of the same sensors in different chambers.

3.2 Recognition algorithm

Using two kinds of recognition algorithm of RBF neural network and SVM[31,32], the recognition models of hydrocarbon gas in bionic electronic nose system were established respectively. By comparing the performance of the two recognition models, the chambers and algorithms which were more suitable for hydro- carbon gas detection and recognition were selected.

Following the characteristics of hydrocarbon gas, the average value (mean) of the entire data set of the electronic nose response curve was extracted as the eigenvalue. According to the data model of bionic electronic nose, a RBF neural network structure with three layers

(six input nodes, three hidden layer nodes, and three output nodes) was constructed, and SVM recognition model was established with the radial basis Eq. (2) with good classification performance and stability as the Kernel function of the support vector machine. The parameter *γ* of the kernel function was determined as 10 by experiment:

$$K(x, y) = \exp(-\gamma \left\| x - y \right\|^2). \qquad (2)$$

10-fold cross validation method was used on 160 sets of valid data for data processing[33] in which the data sets were divided into ten, nine of them was taken as training set and one as verification set. The mean of results of 10 times test was taken as the estimation of the accuracy of the algorithm. Therefore, the data of the 160 groups were divided into 10 groups, and each group has 16 sets of data. 10-fold cross validation was per- formed for 10 times to obtain the average value where the average value of the sensor response was taken as the eigenvalue, and the calculation results were compared with the recognition rate shown in Table 4.

Table 4 Recognition results

Algorithm	RBF		SVM	
Chamber type	Chamber A	Chamber B	Chamber A	Chamber B
Recognition rate	87.11%	91.38%	87.45%	93.14%

For the same recognition algorithm, the recognition rate of chamber B is significantly higher than that of chamber A. For the same chamber, the recognition performance of SVM algorithm is better than that of RBF algorithm. When the average recognition rate was used as the eigenvalue, for the RBF algorithm, the recognition rate of chamber B was 4.27% higher than that of chamber A, for the SVM algorithm, the recognition rate of chamber B was 5.69% higher than that of chamber A. When the number of samples is small, the recognition rate of SVM algorithm is better than that of RBF algorithm.

3.3 3D chamber model and CFD analysis

In order to verify the validity of the bionic composite chamber, the two chambers were compared and analyzed applying fluid mechanics principles. A 3D simulation model of

chamber A and chamber B were established by CATIA software. The model was introduced into mesh software of Gambit for meshing. Fig. 9 is a mesh independent curve for the chamber A and the chamber B at the inlet velocity of 0.8 $m \cdot s^{-1}$. Referring to the curve, the mesh number of the chamber A was determined as 465182, and the mesh number of the chamber B was determined as 511314.

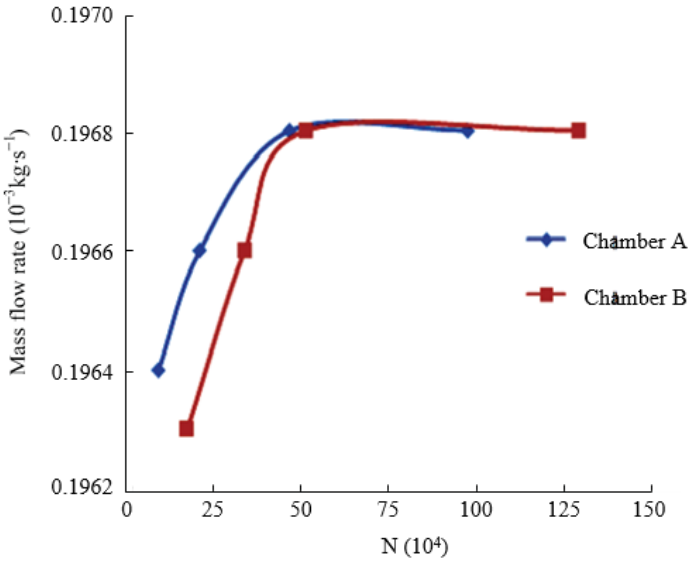

Fig. 9 Change of outlet mass flow rate with mesh number.

The aim of fluid dynamics analysis was mainly to explore the flow of gas in the chamber and the influence of the structure of the electronic nose chamber on its internal gas. The effect of the type of gas can be ignored. Therefore, the dry air was selected as computational fluid, and the inlet velocity was set as the best wind speed 0.8 $m \cdot s^{-1}$:

$$Re = \frac{\rho v d}{\eta}, \qquad (3)$$

where ρ represents the fluid density, v represents the fluid velocity, d represents the cross-sectional diameter, and η represents the viscous coefficient of fluid. The Reynolds number was 832, which can be calculated by Eq. (3). Laminar model was selected and the export condition was selected as free flow. Following the fluid simulation calculation, the CFD-POST software was used for data post-processing. Fig. 10 is the velocity vector diagrams of central

cross-section of the chamber A and the chamber B.

From the velocity vector diagram, it can be seen that after the airflow enters the electronic nose chamber, theCre was a back-flow in the interior and exit of the chamber A, and vortices formed. Due to the addition of the spoiler structure, the generated gas vortices inside the bionic composite chamber B was less than that inside the common chamber A. The flow field inside the chamber was more uniform, so that the sensor array in the chamber B can fully contact with the airflow. This was consistent with the results of Alcitelli *et al*.[34]. Compared with the recognition results, it can be found that the existence of a large number of vortices in the chamber A caused a portion of the gas to remain in the electron nasal chamber, and meanwhile the time for the gas to be measured to reach the sensor surface increased. For the chamber B, due to the existence of bionic structure, the number of vortices in the chamber de- creased, and the time for the gas to reach the sensor surface decreased. This confirmed that the bionic composite chamber B is more favourable than the common chamber A in improving the time cost of electronic nose system detection.

The velocity nephograms of central cross-sections of the chamber A and the chamber B were also obtained by analog simulation. As shown in Fig. 11, the airflow velocity of the inner sensor surface of the bionic composite chamber B was lower than that of the common chamber A. The calculation results of the recognition rate proved that the chamber B was more favourable for the full contact between the gas molecules and the sensor surface than the chamber A, which is helpful for the improvement of signal strength of sensor. This is the main reason that the recognition rate of chamber B was better than that of chamber A for both SVM and RBF algorithms.

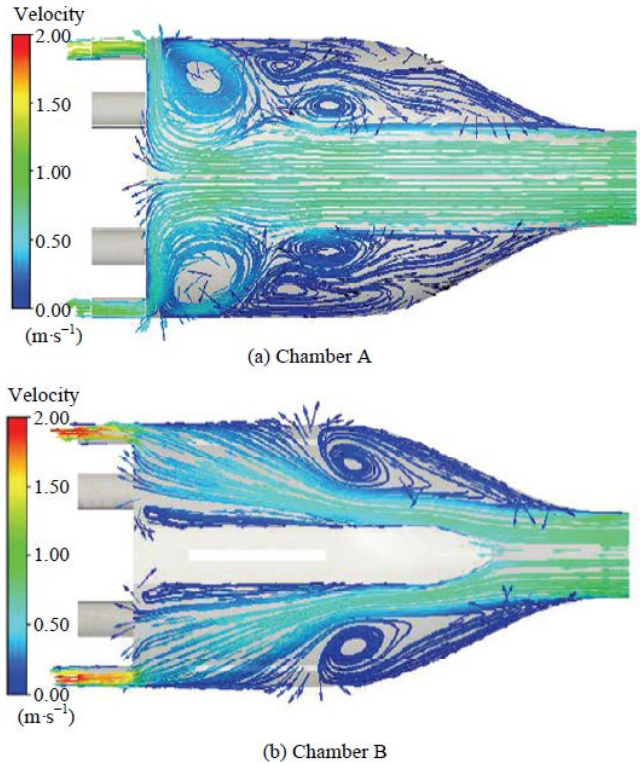

Fig. 10 The velocity vector diagram of central cross-section of electronic nose chambers.

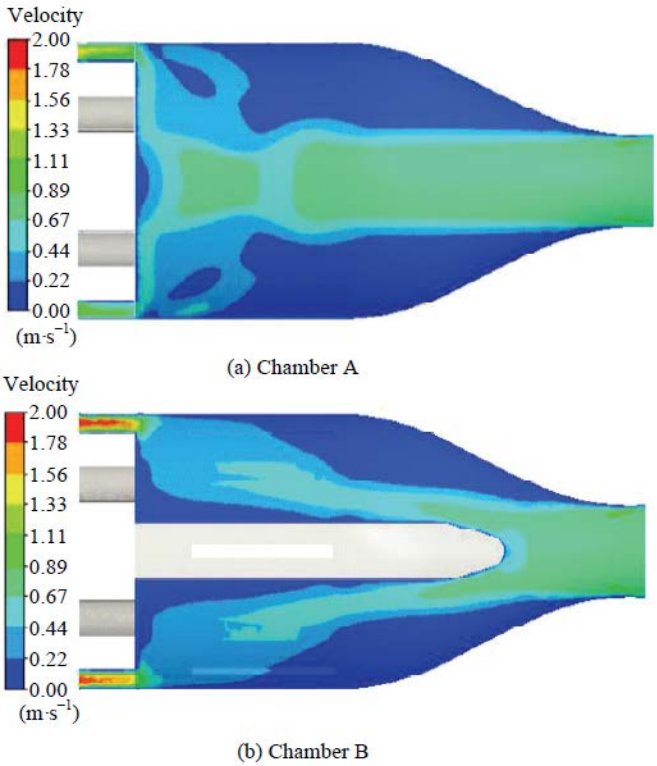

Fig. 11 The velocity nephograms of central cross-sections of electronic nose chambers.

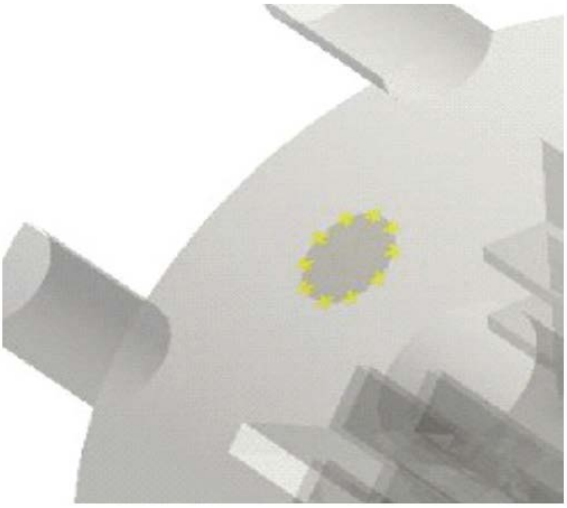

Fig. 12 Sketch map of point location.

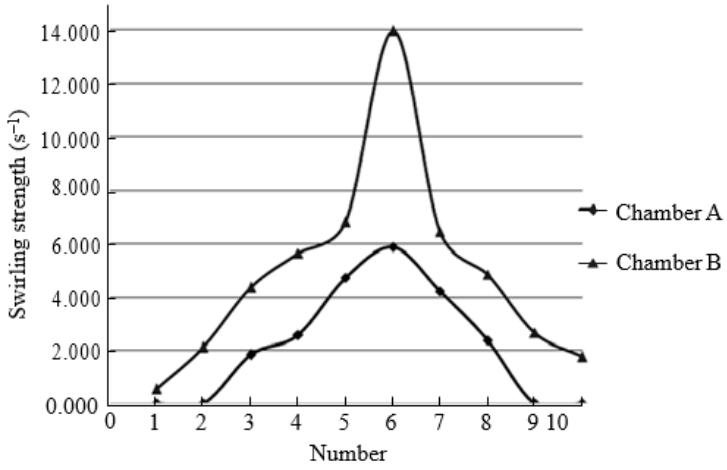

Fig. 13 Comparison of vortex intensity.

Studies by Zhao *et al*.[21,23] showed that small vortices were produced in the olfactory region of the nasal cavity and the vortices can make odorant molecules contact with olfactory cells more fully. Similarly, the sensitivity of the electronic nose will be improved if small vortices are produced around the sensor in the electronic nose chamber. Thus, the gas molecules can fully contact with the surface of the sensor. In this paper, 10 points were chosen on the sensor surface of the chamber A and the chamber B to compare the vortex intensity.

Fig. 12 is the schematic diagram of the position of 10 points taken for analyzing vortex intensity. Fig. 13 shows the comparison of vortex intensity on the sensor surface between

the two chambers. It can be clearly seen from Fig. 13 that the vortex intensity near the sensor in the chamber B was generally larger than that in the chamber A. The calculation results showed that the average vortex intensity near the chamber B sensor was chamber A and the chamber B to compare the vortex intensity.

Fig. 12 is the schematic diagram of the position of 10 points taken for analyzing vortex intensity. Fig. 13 shows the comparison of vortex intensity on the sensor surface between the two chambers. It can be clearly seen from Fig. 13 that the vortex intensity near the sensor in the chamber B was generally larger than that in the chamber A. The calculation results showed that the average vortex intensity near the chamber B sensor was 4.914, and that near the chamber A sensor was 2.166. The vortex intensity near the chamber B sensor was 2.27 times as much as that of the chamber A. This greatly facilitates the odorant molecules to the fully contact with the sensor surface. At the same time, the flow velocity on the surface of chamber B sensor was lower than that on the surface of chamber A, which increases the contact intensity and the contact time between the odorant molecules and the sensor surface. Again, it is proved that the chamber B is superior to the chamber A in the detection accuracy.

4 Conclusion

Based on the structural characteristics of human nasal bone and shark skin, an electronic nose chamber with a bionic composite structure was designed. The related fluid analysis was carried out to verify the validity of the design. The results show that the optimal design of electronic nose chamber was very important for the performance of bionic electronic nose system. For the same sensor array and the same pattern recognition method, the sensitivity of the electronic nose system with the bionic composite chamber was significantly improved compared with that of the common chamber at the optimal inlet velocity. The recognition rate of bionic composite chamber was 4.27% higher than that of common chamber by using RBF algorithm. When the SVM algorithm was used, the recognition rate was in- creased by 5.69%. The results of fluid analysis also verified that the bionic structure inside the optimal bionic composite chamber can reduce the time for gas passing through the non-detection area. The flow rate of the gas on the sensor surface was decreased and the turbulence was increased. It was proved that the spoiler and the bionic composite structure on interior surface of cavity

have positive effect on the airflow disturbance in the chamber. The designed bionic composite chamber can improve the sensitivity of the sensor and the detecCtion performance of bionic electronic nose system.

Acknowledgment

This work was supported by the Key Scientific and Technological Research and Development Projects in Jilin Province (Grant No. 20180201038GX), Jilin Province Development and Reform Commission (Grant Nos. 2016C029 and 2017C051-3), the Education Department of Jilin Province (Grant Nos. [2015] 490, JJKH20170791KJ, JJKH20170812KJ and 20150520075 JH) and the China Postdoctoral Science Foundation (Grant No. 2016M601383).

References

[1] Qin W K, Fan X J, Dong J G. Application of well wall core information in opening oilfields on special high water-contained. *Inner Mongolia Petrochemical Industry*, 2008, **16**, 145–146. (in Chinese)

[2] Gao J, Feng Q N, Sun Y G. Electrode-type complex resistivity logging and its application. *Acta Petrolei Sinica*, 2003, **7**, 62–68. (in Chinese)

[3] Hyperteq L P. *System*, *Method and Apparatus for Mud-gas Extraction*, *Detection and Analysis Thereof*, Patent, US, 2006.

[4] Zhang C, Shi J Y. The factor analysis of affecting the accurate discovery and evaluation of oil gas reservoir in gas logging. *Mud Logging Engineering*, 2001, **12**, 20–23. (in Chinese)

[5] Li Z Y. *Study on Pilot Technology of Gas Separation while Drilling*, Xiamen University, Xiamen, China, 2011. (in Chinese)

[6] Bipan T, Arun J, Animesh M, Devdulal G, Nabarun B, Rajib

[7] B. Electronic nose for black tea quality evaluation by an incremental RBF network. *Sensors and Actuators B*: *Chemical*, 2009, **138**, 90–94.

[8] D'Amico A, Bono R, Pennazza G, Santonico M, Mantini G, Bernabei M, Zarlenga M, Roscioni C, Martinelli E, Paolesse R, Natale C D. Identification of melanoma with a gas sensor array. *Skin Research* & *Technology*, 2008, **14**, 226–236.

[9] Jae H S, Neale H, Erin G, Mark D, Les Z, Michael A. Implementation of an electronic nose for continuous odour monitoring in a poultry shed. *Sensors and Actuators B*: *Chemical*, 2008, **133**, 60–69.

[10] Vito S, Massera E, Piga M, Martinotto L, Francia G D. On field calibration of an electronic nose for benzene estimation in an urban pollution monitoring scenario. *Sensors and Actuators B*: *Chemical*, 2008, **129**, 750–757.

[11] Yang H, Nguyen Q T, Ping Z, Long Y, Hirata Y. Desorption and pervaporation properties of zeolite-filied Poly (dimethylsiloxane) membranes. *Material Research Innovations*, 2001, **5**, 101–106.

[12] Wen J, Inthavong K, Tu J Y, Wang S M. Numerical simulations for detailed airflow dynamics in a human nasal cavity. *Respiratory Physiology* & *Neurobiology*, 2008, **161**,

125–135.

[13] Mösges R, Büchner B, Kleiner M, Freitas R, Hörschler I, Schröder W. Computational fluid dynamics analysis of nasal flow. *B-ENT*, 2010, **6**, 161–165.

[14] Viccione G, Spiniello D, Zarra T, Naddeo V. Fluid dynamic simulation of odour measurement chamber. *Chemical Engineering Transactions*, 2014, **40**, 109–114.

[15] Francesco F D, Falcitelli M, Marano L, Pioggia G. A radially symmetric measurement chamber for electronic noses. *Sensors and Actuators B*: *Chemical*, 2005, **105**, 295–303.

[16] Viccione G, Zarra T, Giuliani S, Naddeo V, Belgiorno V. Performance study of e-nose measurement chamber for environmental odour monitoring. *Chemical Engineering Transactions*, 2012, 109–114.

[17] Yan K, Zhang D. Improving the transfer ability of prediction models for electronic noses. *Sensors and Actuators B*: Chemical, 2015, **220**, 115–124.

[18] Rodriguez-Lujan I, Fonollosa J, Vergara A, Margie H, Ra- mon H. On the calibration of sensor arrays for pattern recognition using the minimal number of experiments. *Chemometrics and Intelligent Laboratory Systems*, 2013, **130**, 123–134.

[19] Lippolis V, Ferrara M, Cervellieri S, Anna D, Filomena E, Michelangelo P, Giancarlo P. Rapid prediction of ochratoxin A-producing strains of Penicillium on dry-cured meat by MOS-based electronic nose. *International Journal of Food Microbiology*, 2015, **218**, 71–77.

[20] Verma P, Yadava R. Polymer selection for SAW sensor array based electronic noses by fuzzy c-means clustering of partition coefficients: Model studies on detection of freshness and spoilage of milk and fish. *Sensors and Actuators B*: *Chemical*, 2015, **209**, 751–769.

[21] Falcitelli M, Benassi A, Francesco F D, Domenici C, Ma- rano L, Pioggia G. Fluid dynamic simulation of a meas- urement chamber for electronic noses. *Sensors and Actuators B*: *Chemical*, 2002, **85**, 166–174.

[22] Waldrop L D, Hann M, Henry A K, Kim A, Punjabi A, Koehl M. Ontogenetic changes in the olfactory antennules of the shore crab, hemigrapsus oregonensis, maintain sniffing function during growth. *Journal of the Royal Society Inter- face*, 2015, **12**, 20141077. Zhao K, Dalton P, Yang G C, Scherer P W. Numerical modeling of turbulent andlaminar airflow and odorant transport during sniffing in the human and rat nose. *Methods*, 2006, **31**, 107–118.

[23] Reznik G K. Comparative anatomy, physiology, and function of the upper respiratory tract. *Environmental Health Perspectives*, 1990, **85**, 171–176.

[24] Zhao K, Scherer P W, Hajiloo S A, Dalton P. Effect of anatomy on human nasal airflow and odorant transport pat- terns: Implications for olfaction. *Chemical Senses*, 2004, **29**, 365–379.

[25] Wen J, Inthavong K, Tu J, Wang S. Numerical simulations for detailed airflow dynamics in a human nasal cavity. *Respiratory Physiology* & *Neurobiology*, 2008, **161**, 125–135.

[26] Ren L Q, Liang Y H. *The Introduction of Bionics*, Science Press, Beijing, China, 2016. (in Chinese)

[27] Jung Y C, Bhushan B. Wetting behavior of water and oil droplets in three-phase interfaces for hydrophobicity/philicity and oleophobicity/philicity. *Langmuir*, 2009, **25**, 14165–14173.

[28] Jiang G L, Xu G. Model of nasal cavity and paranasal si- nuses created for studying the dynamics of the nasal airflow. *Chinese Journal of Otorhinolaryngology Head and Neck Surgery*, 2008, **9**, 665–669. (in Chinese)

[29] Chang Z Y, Chen D H, Men H T, Tong J, Xie J. Electronic nose in chicken freshness detection based on cone-shaped gas chamber bionic technology. *Journal of Jilin University*: *Engineering and Technology Edition*, 2011, **41**, 334–337. (in Chinese)

[30] Zhao D Y, Sun P X, Wang M J, Wang T. Study of replicated technology of micro-riblets on shark skin. *Journal of Dalian University of Technology*, 2015, **52**, 362–366. (in Chinese)

[31] Valdez L F, Gutiérrez J M. Chocolate classification by an electronic nose with pressure controlled generated stimulation. *Sensors*, 2016, **16**, 1745.

[32] Hang L. *Statistics and Learning Methods*, Tsinghua University Press, Beijing, China, 2012, 95–134. (in Chinese)

[33] Zhang H, Yang S, Guo L, Zhao Y, Shao F, Chen F. Comparisons of isomiR patterns and classification performance using the rank-based MANOVA and 10-fold cross-validation. *Gene*, 2015, **569**, 21–26.

[34] Falcitelli M, Benassi A, Francesco F D, Domenici C, Marano L, Pioggia G. Fluid dynamics simulation of a measurement chamber for electronic noses. *Sensors and Actuators B*: *Chemical*, 2002, **85**, 166–174.